THE JOURNAL OF PHYSICAL CHEMISTRY A
A JOURNAL OF THE AMERICAN CHEMICAL SOCIETY

pubs.acs.org/JPCA

Article

Effect of Ligand Attachment at Ag_{11} for CO Oxidation: A Computational Investigation

Deeksha R., Turbasu Sengupta, Deepak Kumar,* and Shiv N. Khanna*

Cite This: *J. Phys. Chem. A* 2023, 127, 10766−10774

Read Online

ACCESS | Metrics & More | Article Recommendations | Supporting Information

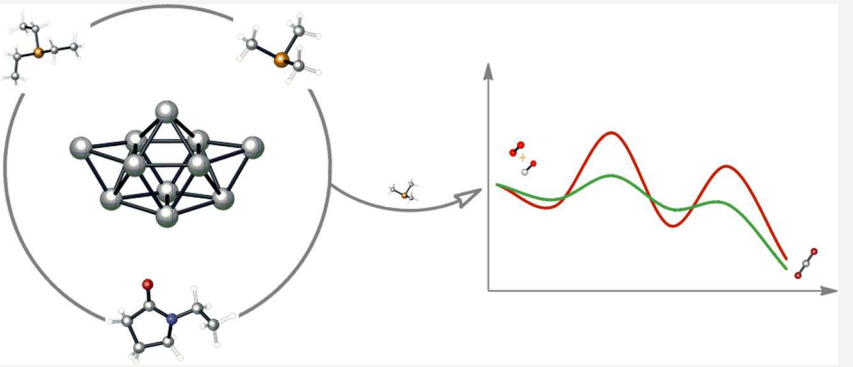

ABSTRACT: Heterogeneous CO oxidation is a demanding reaction at room temperature due to the high activation energy required to break the O=O bond. While several metal clusters are reported to oxidize CO successfully, they fall short of their selectivity for the reaction and recyclability. In this regard, there is a need for economic catalysts with high catalytic activity, low activation barrier, and reusability. In this study, we have investigated the catalytic activity of the neutral pristine and ligated Ag_{11} cluster toward CO oxidation. We investigated the attachment effect of three organic donor ligands: trimethylphosphine, triethylphosphine, and *N*-ethyl pyrrolidone to the Ag_{11} cluster. Our results show that including donor ligands on the Ag_{11} cluster surface can significantly reduce the barrier heights for CO oxidation. The minimum barrier heights with the system coordinated with triethylphosphine showed the lowest activation barrier of 1.06 kcal/mol compared to the high activation barrier of 14.77 kcal/mol recorded for the pristine cluster. Exploration of the reaction mechanism and charge analysis showed that the electron donor ligands activate O_2 via charge donation, thereby reducing the barrier heights of CO oxidation.

INTRODUCTION

In the current industrial revolution era, carbon monoxide (CO) presents a significant threat to humankind. Most CO emissions occur due to the incomplete combustion of fossil fuels in automobiles. Due to its high toxicity and ability to bind strongly with hemoglobin by replacing oxygen, even minor exposure to CO can be lethal. Moreover, being a colorless and odorless gas, exposure to carbon monoxide is difficult to detect or prevent. Chemical conversion of CO to CO_2 is a viable solution to this problem. CO oxidation also has crucial applications in the chemical industry, ranging from catalytic converters, sensing, proton-exchange membrane fuel cells, and synthesizing fossil fuel alternatives. Due to its widespread applications, CO oxidation is one of the most widely studied chemical reactions in the history of heterogeneous catalysis. Although the reaction is exothermic, the oxidation reaction is challenging under ambient conditions due to the high activation energy required to break the strong O=O bond, which also acts as the rate-determining step. Therefore, reducing the O_2 dissociation barrier is a crucial strategy to facilitate the overall CO_2 oxidation process and is the key to designing an effective heterogeneous catalyst. In recent times, metal-based cluster catalysts such as Pt, Rh, Au, Cu, and Ru, either as isolated clusters or supported on various surfaces such as Al_2O_3, ZrO_2, CeO_2, activated carbon, and SiO_2, have been reported with appreciable activity toward CO oxidation.[1−10] However, most of these metals are expensive and also fall short concerning the selectivity toward CO oxidation.[11] Furthermore, Pt-based catalysts are easily deactivated at temperatures of 700−800 °C in the catalytic cycle.[12−14] Therefore, designing cost-effective catalysts with higher activity and selectivity is extremely important.

In the heterogeneous catalytic pathway, CO oxidation can occur in two different ways. First is the Langmuir−Hinshel-

Received: July 12, 2023
Revised: November 19, 2023
Accepted: December 1, 2023
Published: December 14, 2023

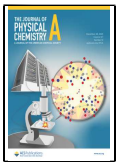

https://doi.org/10.1021/acs.jpca.3c04675
J. Phys. Chem. A 2023, 127, 10766−10774

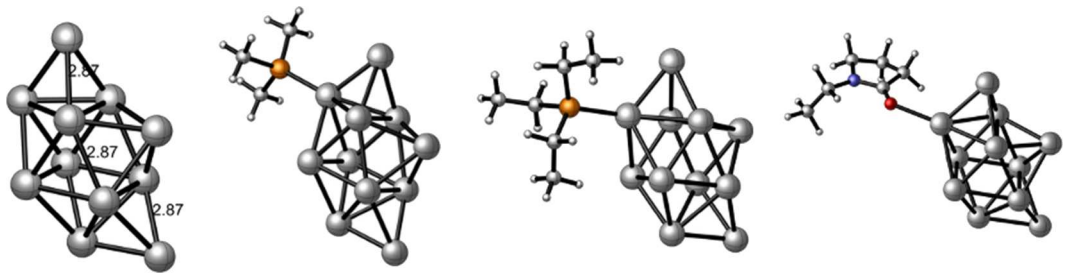

Figure 1. Optimized structures of (left to right) pristine Ag_{11}, PMe_3-coordinated Ag_{11}, PEt_3-coordinated Ag_{11}, and NEP-coordinated Ag_{11} clusters.

wood route, where O_2 and CO molecules are simultaneously adsorbed on the catalyst surface, and CO is subsequently oxidized to CO_2. Second is the Eley−Rideal route, where only O_2 is adsorbed on the catalyst surface, and CO later approaches the surface where the reaction occurs. Numerous theoretical and experimental studies have shown that various forms of silver (free and supported) nanoclusters can successfully catalyze CO oxidation at relatively low temperatures.[15−25] Additionally, theoretical investigations into the structure of Ag nanoclusters have confirmed that the electronic properties of the cluster are predominantly dependent on the presence of the s^1 valence electron.[26,27] Qu et al. reported Ag anchored on mesoporous CeO_2 as efficient catalysts for CO oxidation.[28] It was found that the CeO_2 surface synthesized by the hard template method could carry out 100% CO oxidation at 65 °C, as opposed to the one synthesized via the surfactant-template method, where the required temperature was 150 °C. Similarly, Dutov et al. studied the effect of varying the OH/Ag ratio in silica-supported Ag catalysts at low temperatures for CO oxidation and reported that the highest catalytic activity was observed only at the optimum OH/Ag ratio, where CO_2 was released at room temperature.[29] Motivated by these investigations, we have investigated the potential of pristine and ligated Ag_{11} nanocluster toward CO oxidation in this paper. Nanoclusters and nanoparticles, in general, possess certain unique characteristics that make them better catalysts than their bulk counterparts. The high activity of metal-based nanoclusters can be attributed to the abundantly available surface area, the surplus of free energy, and the ever-changing nature of their surface.[12] Moreover, metal nanoclusters can be fine-tuned to suit desired applications by merely adding or removing a single atom. A notable instance of this is the study reported by Sanchez et al. showing that a gold nanocluster composed of 8 Au atoms is highly active toward CO oxidation, while the one with 7 Au atoms is inactive.[30] Also, detailed computational investigation can be efficiently conducted on nanoclusters to understand the reaction mechanism because of their fixed, finite size.

Despite these advantages, most small-size metal clusters are metastable and prone to dissociation or coalescence. To circumvent this limitation, clusters are usually coated with organic ligands that protect them against dissociation or coalescence. Moreover, ligands also prevent leaching against reactive reagents. Although ligands are usually used for protecting the sensitive core of the cluster, recent investigations have shown that some particular ligands can also be effectively used to alter the redox properties and, thereby, the reactivity. For example, our previous works have shown that organic donor/acceptor ligands can significantly affect the characteristic redox properties of metal-chalcogenide nanoclusters.[31] Coordination of metal clusters with donor phosphine ligands results in an electronic spectrum shift, thereby critically reducing their ionization energies.[32] Attaching multiple donor ligands enables the cluster to behave as superdonors with extremely low first and consecutively lower second and third ionization energies. In another of our recent works, we have shown that the same strategy can be utilized to effectively reduce the barrier heights of CO_2 to formic acid conversion.[33] In this work, we have utilized a similar technique for CO oxidation. We have shown that attaching an electron donor ligand in the vicinity of adsorbed O_2 site of the Ag_{11} cluster significantly reduces barrier heights. For this purpose, we have chosen three organic electron donor ligands, namely, trimethylphosphine (PMe_3), triethylphosphine (PEt_3), and *N*-ethyl pyrrolidone (NEP) and studied the catalytic activity of the ligand-coordinated Ag_{11} cluster. Evaluation of the reaction mechanism by intrinsic bond orbital (IBO) calculations and charge analysis has revealed that the attached donor ligands activate the O_2 molecule via charge donation, thereby facilitating the O_2 dissociation and subsequent C=O bond formation. Our GGA-PBE results show that the CO oxidation barriers can even be reduced to ∼1.0 kcal/mol using suitable donor ligands compared to the 12−15 kcal/mol barrier heights obtained for the pristine cluster. The calculated trend in the barrier heights also qualitatively agrees with the donor strength of the attached ligands. We believe our calculated results reported herewith can aid in designing efficient heterogeneous catalysts for CO oxidation.

■ COMPUTATIONAL METHODS

All Density Functional Theory (DFT) calculations were performed using Gaussian 09[34] quantum chemistry program. Geometry optimizations have been carried out by using the PBE[35] functional. The LANL2DZ[36] basis set was used for the silver atoms, and the TZVP[37] basis set was used for Carbon, Oxygen, Phosphorus, and Hydrogen. Vibrational frequency analysis was conducted to confirm that the optimized structures are local minima. The transition states were identified using the Berny[38] algorithm with the GEDIIS[39] method and were characterized by a single imaginary frequency. Hirshfeld charge analysis[40] and natural population analysis[41] (NPA) were carried out to understand the mechanism of charge transfer between the ligand and the cluster. Intrinsic reaction coordinates (IRC) calculations[42] were also performed for both the transition states of the pristine cluster to ensure that they connected the corresponding intermediates and products along the potential energy surface (PES). The density of states (DOS) calculation was performed with Multiwfn,[43] and the reaction mechanism was evaluated by intrinsic bond orbital (IBO) calculations by using the IboView software.[44,45]

https://doi.org/10.1021/acs.jpca.3c04675
J. Phys. Chem. A 2023, 127, 10766−10774

RESULTS AND DISCUSSION

In the present study, we look at the pristine Ag_{11} cluster and the effect of ligation by trimethylphosphine (PMe_3), triethylphosphine (PEt_3), and *N*-ethyl-2-pyrrolidone (NEP) on the same toward CO oxidation. The starting geometry of the cluster was adapted from McKee and Samokhvalov, where the structures were optimized at the M06 level, and the ECP28MWB basis set was employed for Ag.[46] Our choice of Ag_{11} is motivated by recent experiments that have identified stable ligated Ag_{11} clusters via mass spectroscopy of ligated species.[31,47−49] Clusters within such a size range are well-known for dominant electronic and geometric effects which usually lead to unique reactivity. Since the present work is focused on the effect of ligands on the reactivity of clusters, Ag_{11} was a natural choice. The optimized structures shown in Figure 1 appear to be in general agreement with previously reported results. The average distance between two Ag atoms was found to be 2.87 Å. Several different attachment positions for O_2 and CO were investigated to arrive at the lowest attainable minima. Furthermore, in the process of finding the lowest achievable minima, different spin multiplicities (2, 4, 6, 8, and 10) were optimized for $Ag_{11,}$ and the lowest energy minima, i.e., the doublet, was chosen. The optimized ground state geometry along with some important interatomic distances, are shown in Figure 2a. The molecular orbital

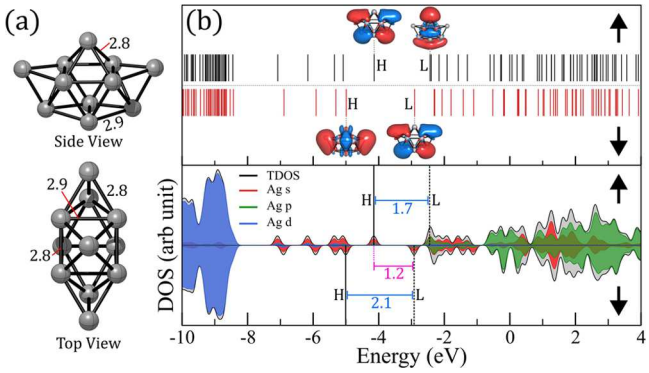

Figure 2. (a) Side view and top view of optimized pristine Ag_{11} cluster, (b) DOS plot of optimized pristine Ag_{11} cluster.

(MO) and density of states (DOS) diagram for both spin channels are included in Figure 2b. Additionally, The HOMO−LUMO isosurfaces and the gaps for both the spin channels are also marked. The DOS diagram reveals that the HOMO orbitals for both spins are mostly composed of s orbitals of Ag, along with minor contributions from p and d orbitals. The optimized energies of the various multiplicities are reported in Supporting Information (Table S1). At every step, the absence of any imaginary frequency was ensured, and all the structures in the study were taken at their local minima. It was observed that the O_2 molecule preferred to bind with Ag_{11} in a diagonally perpendicular manner, as depicted in Figure 3, and showed a bond distance of 2.38 Å with Ag. Initially, the bond length of the O_2 molecule adsorbed on the Ag_{11} cluster was found to be 1.29 Å; and this was increased to 1.30 ± 0.01 Å upon optimization with CO alongside. The binding energy analysis was conducted, and the most thermodynamically favorable binding sites for both O_2 and CO were chosen.

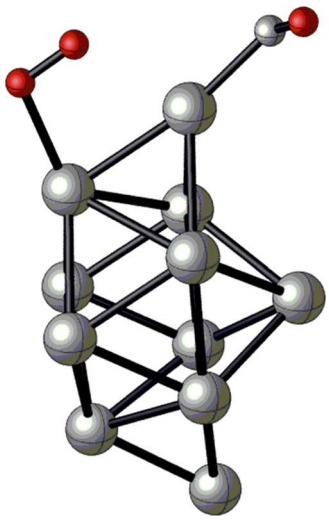

Figure 3. Optimized pristine Ag_{11} cluster showing the adsorption sites and orientation of O_2 and CO.

CO oxidation can occur on a catalyst surface via the Langmuir−Hinshelwood (LH) pathway or the Eley−Rideal (ER) pathway.[50,51] In this study, we have confirmed the Langmuir−Hinshelwood mechanism for CO oxidation. In the case of surface catalysts, the ER mechanism is generally preferred due to a low activation barrier; however, in the case of metal and metal oxide clusters, the LH mechanism is preferred.[52−56] Due to the stronger binding energy between the substrate and the reactant molecules, namely, O_2 and CO, the LH pathway is generally avoided in surface catalysis. In the ER mechanism, only O_2 is chemisorbed on the catalyst surface, whereas in the LH mechanism, an additional CO molecule is adsorbed along with O_2. The stronger the binding energy between the adsorbate and the surface, the higher will be the reaction barrier. Furthermore, in the ER pathway, the transition state can be attained by weakening the bond between the oxygen and the metal atoms, and in the LH pathway, the second transition state can be attained by weakening an additional bond between the CO molecule and the surface. However, the ER pathway requires the CO to be adsorbed by making a certain angle with the cluster. This is often not the case, as the CO molecule tends to enter a chemisorption well[53] when it adsorbs on the cluster, and the probability of this occurring is fairly high. Even if the initial desirable orientation for the ER mechanism is achieved, it may not proceed further because the activation barrier will be significantly high when CO approaches O_2. Hence, the ER pathway is restricted to surface catalysts. It is worth mentioning that the pathway that leads to the highest O_2 activation will be chosen.

In the LH mechanism, O_2 and CO molecules are simultaneously adsorbed onto the Ag_{11} cluster, and they subsequently react to produce CO_2. Several studies have confirmed the successful possibilities of O_2 and CO adsorption on supported and surface Ag catalysts and their activation on the same.[5,57−60] The reaction of CO oxidation begins with the simultaneous adsorption of O_2 and CO on the Ag_{11} cluster. All the possible sites on the Ag_{11} cluster were investigated for the adsorption of O_2 and CO molecules, and the site that resulted in the lowest energy and the most effective in activating O_2 activation was chosen. Among the various sites explored, bridge-like adsorption of O_2 was avoided to maintain free

https://doi.org/10.1021/acs.jpca.3c04675
J. Phys. Chem. A 2023, 127, 10766−10774

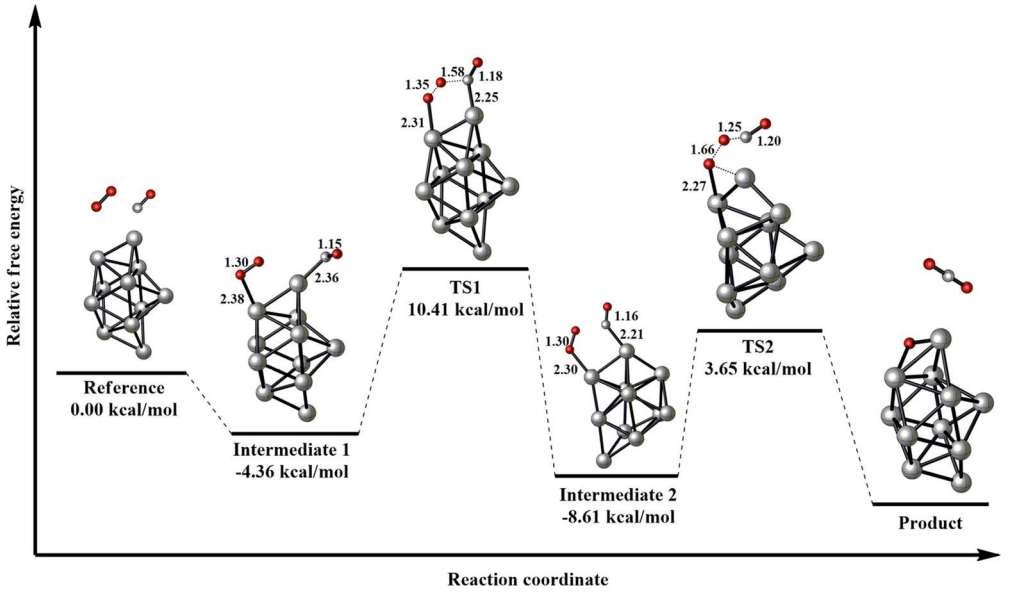

Figure 4. Reaction profile of CO oxidation on pristine Ag_{11} cluster.

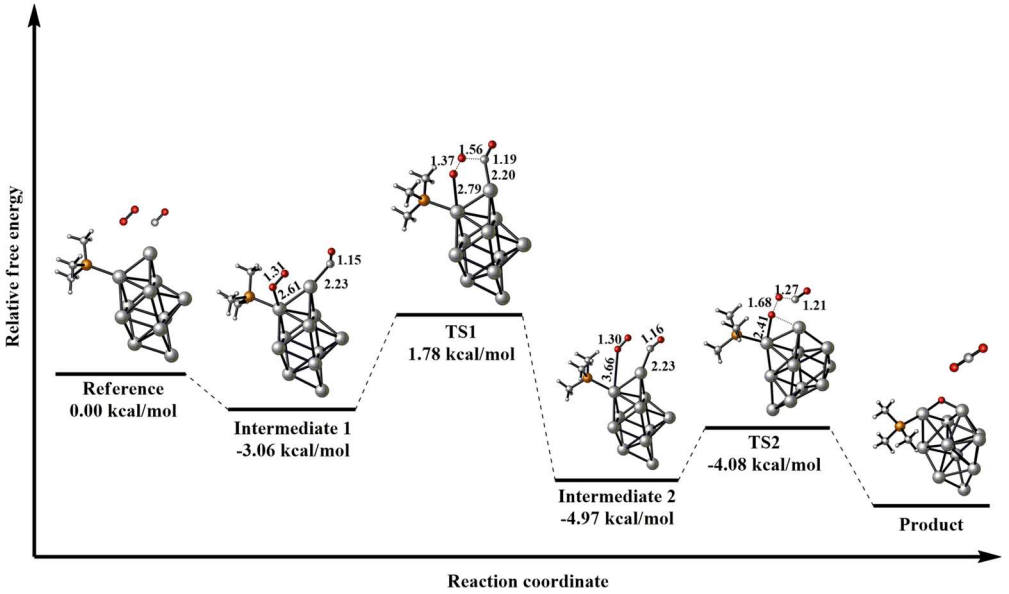

Figure 5. Reaction profile of CO oxidation on Ag_{11}−PMe_3 cluster.

active sites on the catalyst. Upon adsorption, O_2 is activated, leading to the formation of the first intermediate. Subsequently, the first transition state is formed, which includes the simultaneous weakening of the O_2 bond and the beginning of the formation of CO_2. Next, there is an increase in the O=O length and a decrease in the newly formed bond between O_2 and CO in the second intermediate. Finally, there is a complete breakage of O_2 and the complete formation of CO_2, which is achieved via the second transition state. This mechanism was found to be consistent for CO oxidation even when the three ligands, PMe_3, PEt_3, and NEP, were coordinated with the pristine Ag_{11} cluster. Our investigation shows that the electron donor ligands are most effective in reducing the barrier heights when attached adjacent to the CO site, hence, in this work, we have considered such sites for attaching all three donor ligands. The adsorption of O_2 on the ligand-coordinated cluster was not found to be significantly different, as the O_2 molecule bonded with the cluster with a distance of 2.61 Å in the case of both PMe_3 and PEt_3 and 2.34 Å in the case of NEP.

We calculated the activation barrier for the formation of the O−O−C-O intermediate in the case of the pristine Ag_{11} cluster, as well as the ligand-coordinated clusters (Figures 4−7). With respect to transition state 1 (TS-1), we observed that the activation barrier was 14.77 kcal/mol, 4.85, 1.06, and 1.72 kcal/mol with pristine Ag_{11} cluster, PMe_3 coordinated cluster, PEt_3 coordinated cluster, and NEP coordinated cluster, respectively. The drastic drop in the activation barrier when Ag_{11} is coordinated with the ligands suggests that the ligands significantly affect the reaction. The PEt_3-coordinated system showed the lowest activation barrier. Furthermore, it was observed that while all the ligands bond with the Ag_{11} cluster at the same site, in the case of NEP, the reactant O_2 molecule is pushed away from the ligand-binding site. This can be attributed to the repulsion between NEP and the O_2 molecule

https://doi.org/10.1021/acs.jpca.3c04675
J. Phys. Chem. A 2023, 127, 10766−10774

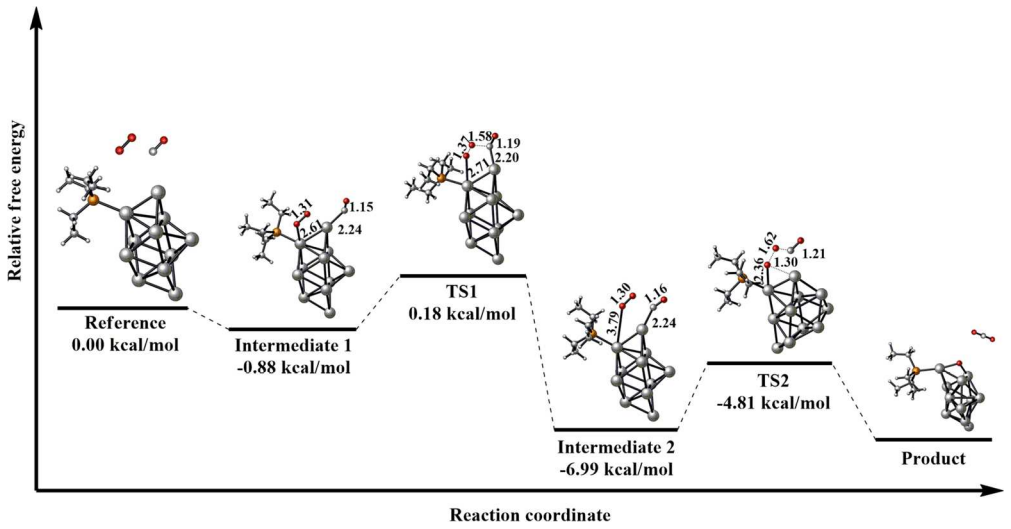

Figure 6. Reaction profile of CO oxidation on Ag_{11}−PEt_3 cluster.

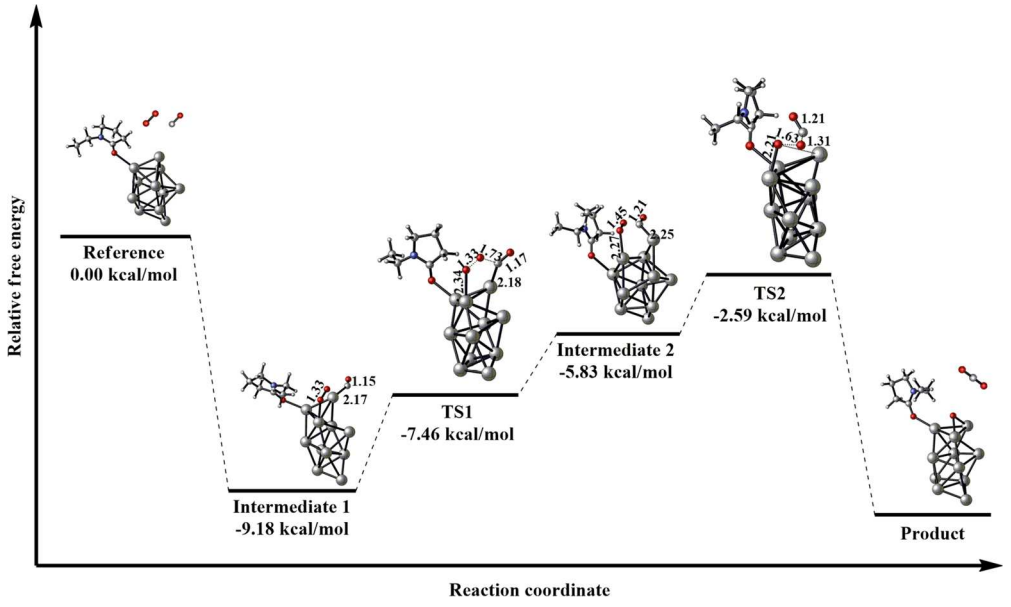

Figure 7. Reaction profile of CO oxidation on Ag_{11}−NEP cluster.

caused by the former's bulkiness. Unlike the other systems, the charge donation in the case of NEP is not immediate from the ligand to the cluster to the reactant O_2 molecule. Hence, the slightly higher barrier in the case of the NEP-coordinated system can be attributed to the fact that the sites of ligation and reaction are different. The calculated activation barriers for all the clusters are summarized in Table 1. Additionally, to address the possibility of ligand oxidation preceding CO oxidation, we investigated the oxidation cycle of the ligands using Ag_{11}−PMe_3 as a representative system. In this instance, the calculated activation barrier of 24.02 kcal/mol was significantly higher than any of the barriers observed for CO oxidation. Based on these findings, we conclude that CO oxidation is the favored pathway over ligand oxidation. This reaction profile is provided in the Supporting Information (Figure S5).

Table 1. Summary of Calculated Activation Barriers

cluster	first activation energy barrier (kcal/mol)	second activation energy barrier (kcal/mol)
pristine Ag_{11}	14.77	12.26
Ag_{11}−PMe_3	4.85	0.90
Ag_{11}−PEt_3	1.06	2.19
Ag_{11}−NEP	1.72	3.24

We would like to briefly outline the effect of ligands on the cluster. The ligands interact with the cluster, forming charge-transfer complexes. As our previous studies have indicated, two kinds of effects are responsible for altering the ionization energy; initial state effects and final state effects. Initial state effects arise primarily via the formation of bonding and antibonding orbitals that cause a shift in the HOMO level. Final state effects arise from the improved binding of the electron-donating ligands with the nanocluster.[31] All the ligands studied here are electron-donating in nature and create surface dipoles that cause a reduction in the ionization energy of the system. This effect is somewhat similar to the

https://doi.org/10.1021/acs.jpca.3c04675
J. Phys. Chem. A 2023, 127, 10766−10774

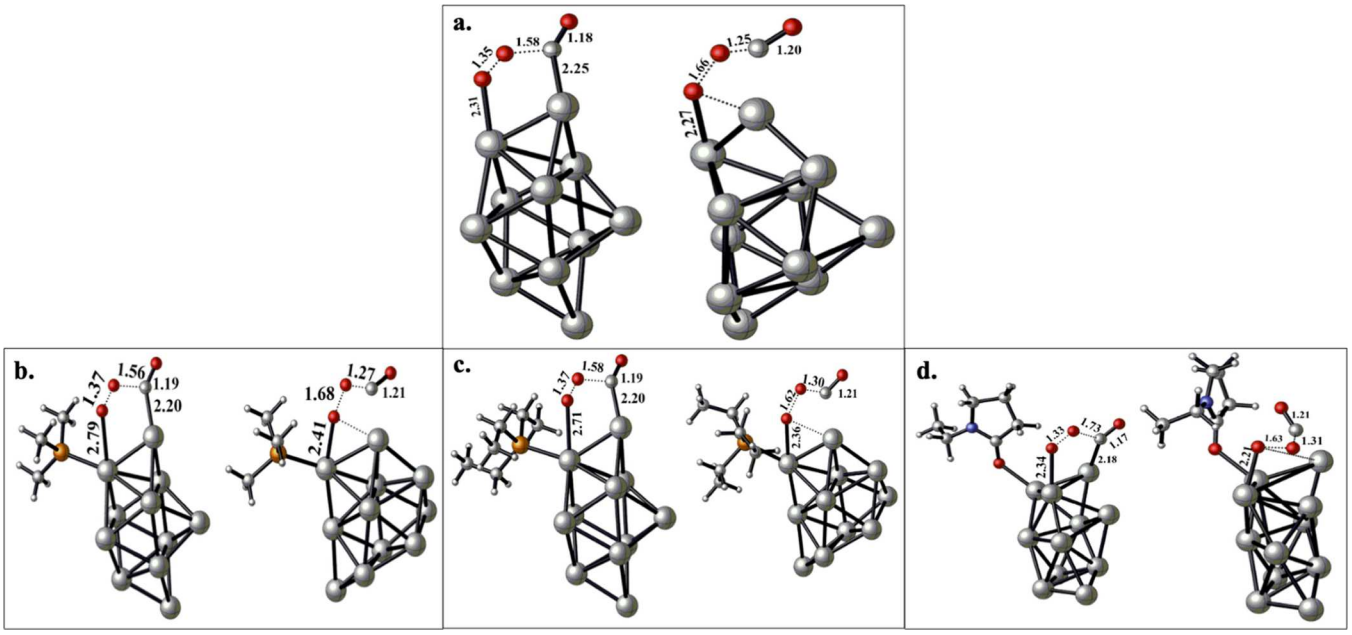

Figure 8. Transition state structures (left-TS1) and (right-TS2) of (a) pristine Ag_{11}, (b) Ag_{11}−PMe_3, (c) Ag_{11}−PEt_3, and (d) Ag_{11}−NEP.

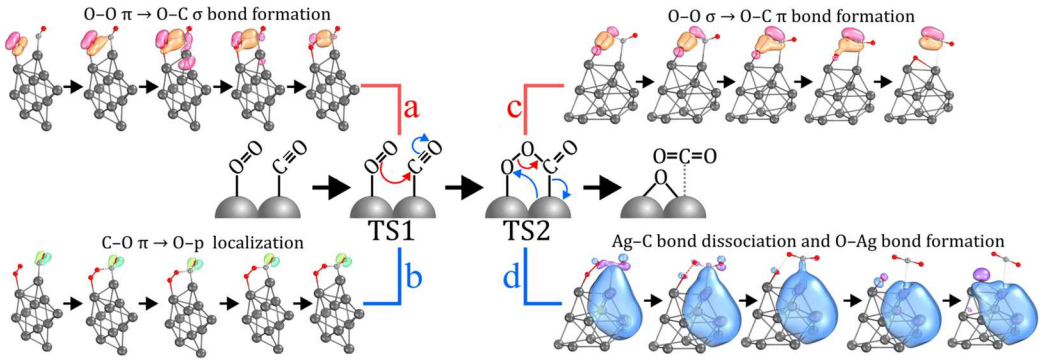

Figure 9. IBO analysis for TS1 and TS2. In (a), the migration of the orange lobe signifies the conversion of the π bond of O_2 and the subsequent formation of the O−C σ bond in TS1. In (b), the shift of both the green and blue regions signifies the localization of the coordinate-covalent bond of CO on O. In (c), the σ orbital of O_2 converts to form the π bond of CO_2 in TS2, shown in pink and orange. In (d), the electron localization shown in blue leads to the dissociation of Ag−C, causing CO_2 to split.

adjustment caused by dipole moment on the work function of a metal.[61−65] While interacting with the cluster, the ligands establish bonds with the surface sites, creating bonding and antibonding orbitals, and when the antibonding orbitals are filled, a rise in the energy of the hybridized HOMO is observed. This leads to an easier transition of electrons from the lower energy state to the excited energy state.

The initial bond length of O_2 in the reactant state was found to be 1.24 Å with all the systems, pristine Ag_{11}, as well as all the three ligand-coordinated clusters. In the case of the pristine Ag_{11} system, the O_2 bond activation in the first transition state is found to be 1.35 Å, and subsequently reaches 1.66 Å in the second transition state (Figure 8a). With PMe_3-coordinated cluster, the initial activation in the first transition state is 1.37 Å, and elongates up to 1.68 Å in the second transition state (Figure 8b). With PEt_3-coordinated cluster, the first transition state showed an O_2 activation of 1.37 Å, and 1.62 Å in the second (Figure 8c). Finally, with the NEP-coordinated system, O_2 activation shows a bond length of 1.33 Å in the first transition state and 1.63 Å in the second transition state (Figure 8d). The PMe_3-coordinated cluster showed the highest O_2 activation. While all the ligands are electron-donating, the activation is highest in the case of PMe_3 owing to the higher inductive effect of the methyl group. Additionally, due to the electronegativity of the oxygen in NEP, the O_2 activation is marginally lower. It is worth noting that successive ligand attachment was investigated, and since there was no significant change in the activation barrier in the case of 2-PMe_3, it was not pursued further.

To further quantify the donation of charge upon ligation, we have carried out Hirshfeld charge analysis. As previously indicated, when an electron-donating ligand is attached to the pristine Ag_{11} cluster, there is a donation of charge from the ligand to the cluster, which then passes the charge to the oxygen molecule, thereby activating it. To confirm this phenomenon, we calculated the Hirshfeld charge. We found that the charge on the O atom of Ag−O in the pristine Ag_{11} cluster was −0.146 in the first intermediate, and upon attaching PMe_3, it decreased to −0.210 in the first transition state, indicating that there was a transfer of charge from the cluster to the O atom. Furthermore, the charge on the O atom of Ag−O in the first transition state geometries was found to

https://doi.org/10.1021/acs.jpca.3c04675
J. Phys. Chem. A 2023, 127, 10766−10774

increase to −0.211 and −0.173 in the case of PEt_3- and NEP-coordinated clusters, respectively. As the reaction proceeds from the intermediate to the first transition state geometry, we noted that the charge donation is most significant in the case of PEt_3, leading to the lowest activation barrier. The charge on the O atom of Ag−O decreased from −0.174 in the first intermediate to −0.211 in the first transition state, accounting for the drop in the barrier. However, in the case of PMe_3 and NEP, there was no significant charge donation between P and Ag, and O and Ag respectively. The summary of the Hirshfeld charge analysis is provided in the Supporting Information (Tables S2−S5). The same charge transfer analysis was also tested by natural population analysis (NPA) to confirm the consistent results, whose details are provided in the Supporting Information (Tables S6−S9).

To further understand the reaction mechanism of CO oxidation on the Ag_{11} cluster, we have performed the intrinsic bond orbital (IBO) calculations on the geometries along the intrinsic reaction coordinate (IRC). It is well-known that identifying the energetic and geometric alteration of intrinsic bond orbitals along a reaction pathway can establish the mechanism of any unknown or complex reaction process.[44,45] Since the optimized structures of transition states and intermediates remain largely similar even after ligand attachment, we can conclude that the reaction mechanism of CO oxidation on the Ag_{11} cluster is unaltered upon ligand attachment. As a result, the IBO calculations were performed only for the CO oxidation pathway on the pristine Ag_{11} cluster. The calculated results of the IRC calculations for both transition states are included in the Supporting Information (Figures S1 and S2). As shown in Figure 9, we have summarized the IBO calculation results. As noted before, the CO → CO_2 oxidation pathway on the Ag_{11} cluster proceeds via two transition states (TS1 and TS2). IBO calculation reveals that in the reaction pathway of the first transition state (TS1), the O=O π bond is converted to O−C σ bond (shown in Figure 9a), resulting in a subsequent localization of the coordinate covalent π bond of the carbon monoxide to the O atom (Figure 9b). The σ bond of O_2 gets dissociated during the second transition state (Figure 9c). During this pathway, the O−O σ bond is seen to convert to the C−O π bond of carbon dioxide. Subsequent electron delocalization leads to the dissociation of the C−Ag bond, which is followed by the formation of a new O−Ag bond on the cluster surface (Figure 9d). As a result of the C−Ag bond dissociation, the CO_2 molecule gets free from the surface, and the newly formed O−Ag bond results in an Ag−O−Ag bridge configuration in the product, as shown earlier. It is important to note here that the presence of a residual oxygen atom does not imply an incomplete reaction. Upon the generation and subsequent desorption of CO_2, a single cycle of CO oxidation attains a state of completion. This pivotal step within a given cycle subsequently serves as the inception point for the ensuing reaction sequences. The lingering O atom assumes a catalytic role, facilitating additional oxidation reactions, or it may engage in recombination with other oxygen atoms to generate O_2, thereby initiating another cycle of the process. To validate this hypothesis, we further investigated the second catalytic cycle between a CO molecule and the residual oxygen for both the pristine Ag_{11} cluster and the Ag_{11}−PMe_3 cluster. The latter was chosen as a representative for all the three ligands employed in this study. In the case of the pristine cluster, a barrier of 16.28 kcal/mol was observed. For the ligated cluster, the barrier was found to be 1.24 kcal/mol. These reaction profiles are provided in the Supporting Information (Figure S3 and Figure S4).

CONCLUSIONS

We have conducted density functional calculations to understand the catalytic activity of Ag_{11} toward CO oxidation. Subsequently, three different organic donor ligands, PMe_3, PEt_3, and NEP, were coordinated to the pristine Ag_{11} cluster, and their activity with respect to CO oxidation was studied. While the pristine system showed an activation barrier of 14.77 kcal/mol, attaining the first transition state, the PEt_3-stabilized cluster showed the least barrier of 1.06 kcal/mol. Further, all the transition states obtained in the study were validated using IRC, and the highest O_2 activation was seen in both PMe_3 and PEt_3, wherein a change from 1.31 to 1.68 Å and 1.62 Å respectively was observed compared to the pristine cluster (1.35 Å). In addition, IBO analysis of the IRC calculations was performed for the pristine cluster to understand the mechanism of the reaction. It was observed in TS1, that the π bond of O=O is transformed into a σ bond between the O of O_2 and the C of CO. Later, in TS2, the σ bond between O−O is broken to form the π bond of O=C=O. The significant drop in the activation barrier upon coordination with ligands can be attributed to the synergistic stabilization effect of electron donation by the ligands and the generation of surface dipoles that reduce the ionization energy of the metal cluster, leading to a reduction in the HOMO−LUMO gap of the metal, which in turn induces electron transfer from the metal to oxygen, activating it. The activated oxygen subsequently reacts with the CO, forming CO_2. The slightly higher activation barrier with NEP is explained by considering the presence of oxygen, an electronegative element, which changes the site of reaction by pushing the O_2 away from the ligation site. Hirshfeld charge analysis and NPA further confirmed the charge transfer from the ligands to the cluster, resulting in the donation of charge from the cluster to the adsorbed O_2 molecule, activating it. This study helps to understand in detail the mechanism of CO oxidation followed on Ag_{11} metal cluster and the role of electron-donating organic ligands in reducing the activation barrier of the reaction.

ASSOCIATED CONTENT

Supporting Information

The Supporting Information is available free of charge at https://pubs.acs.org/doi/10.1021/acs.jpca.3c04675.

Optimized energies, optimized coordinates, IRC pathways, Hirshfeld charge analysis, and natural population analysis (PDF)

AUTHOR INFORMATION

Corresponding Authors

Deepak Kumar − *Department of Chemistry, Faculty of Mathematical and Physical Sciences, M.S. Ramaiah University of Applied Sciences, Bengaluru, Karnataka 560058, India;* orcid.org/0000-0002-4683-5084; Email: kumar.deep1467@gmail.com

Shiv N. Khanna − *Physics Department, Virginia Commonwealth University, Richmond, Virginia 23284-2000, United States;* orcid.org/0000-0002-9797-1289; Email: Snkhanna@vcu.edu

https://doi.org/10.1021/acs.jpca.3c04675
J. Phys. Chem. A 2023, 127, 10766−10774

Authors

Deeksha R. − *Department of Chemistry, Faculty of Mathematical and Physical Sciences, M.S. Ramaiah University of Applied Sciences, Bengaluru, Karnataka 560058, India*

Turbasu Sengupta − *Physics Department, Virginia Commonwealth University, Richmond, Virginia 23284-2000, United States*

Complete contact information is available at: https://pubs.acs.org/10.1021/acs.jpca.3c04675

Author Contributions

The manuscript was written through the contributions of all authors. All authors have approved the final version of the manuscript. All the authors have contributed equally.

Notes

The authors declare no competing financial interest.

■ ACKNOWLEDGMENTS

D.R. acknowledges DST-SERB, India for providing a junior research fellowship. D.K. acknowledges DST-SERB, India for providing financial support (CRG/2020/003882). T.S. and S.N.K. thank the National Science Foundation (CHE-1900094) for the support of this work.

■ REFERENCES

(1) Bulushev, D. A.; Yuranov, I.; Suvorova, E. I.; Buffat, P. A.; Kiwi-Minsker, L. Highly Dispersed Gold on Activated Carbon Fibers for Low-Temperature CO Oxidation. *J. Catal.* **2004**, *224* (1), 8−17.

(2) Jia, C.-J.; Schwickardi, M.; Weidenthaler, C.; Schmidt, W.; Korhonen, S.; Weckhuysen, B. M.; Schüth, F. Co_3O_4 − SiO_2 Nanocomposite: A Very Active Catalyst for CO Oxidation with Unusual Catalytic Behavior. *J. Am. Chem. Soc.* **2011**, *133* (29), 11279−11288.

(3) Bera, P.; Gayen, A.; Hegde, M. S.; Lalla, N. P.; Spadaro, L.; Frusteri, F.; Arena, F. Promoting Effect of CeO_2 in Combustion Synthesized Pt/CeO_2 Catalyst for CO Oxidation. *J. Phys. Chem. B* **2003**, *107* (25), 6122−6130.

(4) Joo, S. H.; Park, J. Y.; Renzas, J. R.; Butcher, D. R.; Huang, W.; Somorjai, G. A. Size Effect of Ruthenium Nanoparticles in Catalytic Carbon Monoxide Oxidation. *Nano Lett.* **2010**, *10* (7), 2709−2713.

(5) Liu, J.-H.; Wang, A.-Q.; Chi, Y.-S.; Lin, H.-P.; Mou, C.-Y. Synergistic Effect in an Au−Ag Alloy Nanocatalyst: CO Oxidation. *J. Phys. Chem. B* **2005**, *109* (1), 40−43.

(6) Nikolaev, S. A.; Golubina, E. V.; Krotova, I. N.; Shilina, M. I.; Chistyakov, A. V.; Kriventsov, V. V. The Effect of Metal Deposition Order on the Synergistic Activity of Au−Cu and Au−Ce Metal Oxide Catalysts for CO Oxidation. *Applied Catalysis B: Environmental* **2015**, *168−169*, 303−312.

(7) Zhang, X.; Wang, H.; Xu, B.-Q. Remarkable Nanosize Effect of Zirconia in Au/ZrO_2 Catalyst for CO Oxidation. *J. Phys. Chem. B* **2005**, *109* (19), 9678−9683.

(8) Park, J. Y.; Zhang, Y.; Grass, M.; Zhang, T.; Somorjai, G. A. Tuning of Catalytic CO Oxidation by Changing Composition of Rh−Pt Bimetallic Nanoparticles. *Nano Lett.* **2008**, *8* (2), 673−677.

(9) Gustafson, J.; Westerström, R.; Balmes, O.; Resta, A.; van Rijn, R.; Torrelles, X.; Herbschleb, C. T.; Frenken, J. W. M.; Lundgren, E. Catalytic Activity of the Rh Surface Oxide: CO Oxidation over Rh(111) under Realistic Conditions. *J. Phys. Chem. C* **2010**, *114* (10), 4580−4583.

(10) Ivanova, A. S.; Slavinskaya, E. M.; Gulyaev, R. V.; Zaikovskii, V. I.; Stonkus, O. A.; Danilova, I. G.; Plyasova, L. M.; Polukhina, I. A.; Boronin, A. I. Metal−Support Interactions in Pt/Al2O3 and Pd/Al2O3 Catalysts for CO Oxidation. *Applied Catalysis B: Environmental* **2010**, *97* (1−2), 57−71.

(11) Huang, Y.; Wang, A.; Wang, X.; Zhang, T. Preferential Oxidation of CO under Excess H2H2 Conditions over Iridium Catalysts. *Int. J. Hydrogen Energy* **2007**, *32* (16), 3880−3886.

(12) Newton, M. A. Dynamic Adsorbate/Reaction Induced Structural Change of Supported Metal Nanoparticles: Heterogeneous Catalysis and Beyond. *Chem. Soc. Rev.* **2008**, *37* (12), 2644.

(13) Nanda, K. K.; Maisels, A.; Kruis, F. E.; Fissan, H.; Stappert, S. Higher Surface Energy of Free Nanoparticles. *Phys. Rev. Lett.* **2003**, *91* (10), No. 106102.

(14) Cao, A.; Lu, R.; Veser, G. Stabilizing Metal Nanoparticles for Heterogeneous Catalysis. *Phys. Chem. Chem. Phys.* **2010**, *12* (41), 13499.

(15) Carabineiro, S. A. C.; Tavares, P. B.; Figueiredo, J. L. Gold on Oxide-Doped Alumina Supports as Catalysts for CO Oxidation. *Appl. Nanosci* **2012**, *2* (1), 35−46.

(16) Manzoor, D.; Pal, S. Reactivity and Catalytic Activity of Hydrogen Atom Chemisorbed Silver Clusters. *J. Phys. Chem. A* **2015**, *119* (24), 6162−6170.

(17) Socaciu, L. D.; Hagen, J.; Roux, J. L.; Popolan, D.; Bernhardt, T. M.; Wöste, L.; Vajda, Š. Strongly Cluster Size Dependent Reaction Behavior of CO with O2 on Free Silver Cluster Anions. *J. Chem. Phys.* **2004**, *120* (5), 2078−2081.

(18) Wang, L.-N.; Li, X.-N.; He, S.-G. Recent Research Progress in the Study of Catalytic CO Oxidation by Gas Phase Atomic Clusters. *Sci. China Mater.* **2020**, *63* (6), 892−902.

(19) Zeng, W.; Tang, J.; Wang, P.; Pei, Y. Density Functional Theory (DFT) Studies of CO Oxidation Reaction on M_{13} and $Au_{18}M$ Clusters (M = Au, Ag, Cu, Pt and Pd): The Role of Co-Adsorbed CO Molecule. *RSC Adv.* **2016**, *6* (61), 55867−55877.

(20) Falsig, H.; Hvolbæk, B.; Kristensen, I. S.; Jiang, T.; Bligaard, T.; Christensen, C. H.; Nørskov, J. K. Trends in the Catalytic CO Oxidation Activity of Nanoparticles. *Angew. Chem., Int. Ed.* **2008**, *47* (26), 4835−4839.

(21) Zhou, J.; Li, Z.-H.; Wang, W.-N.; Fan, K.-N. Density Functional Study of the Interaction of Carbon Monoxide with Small Neutral and Charged Silver Clusters. *J. Phys. Chem. A* **2006**, *110* (22), 7167−7172.

(22) Bernhardt, T. M.; Socaciu-Siebert, L. D.; Hagen, J.; Wöste, L. Size and Composition Dependence in CO Oxidation Reaction on Small Free Gold, Silver, and Binary Silver−Gold Cluster Anions. *Applied Catalysis A: General* **2005**, *291* (1−2), 170−178.

(23) Kim, Y. D.; Ganteför, G.; Sun, Q.; Jena, P. Chemisorption of Atomic and Molecular Oxygen on Au and Ag Cluster Anions: Discrimination of Different Isomers. *Chem. Phys. Lett.* **2004**, *396* (1−3), 69−74.

(24) Hammer, B.; Morikawa, Y.; Nørskov, J. K. CO Chemisorption at Metal Surfaces and Overlayers. *Phys. Rev. Lett.* **1996**, *76* (12), 2141−2144.

(25) Dholabhai, P. P.; Wu, X.; Ray, A. K. An Ab Initio Study of the Use of for Catalytic Oxidation of CO. *Journal of Molecular Structure: THEOCHEM* **2005**, *723* (1−3), 139−145.

(26) Ho, J.; Ervin, K. M.; Lineberger, W. C. Photoelectron Spectroscopy of Metal Cluster Anions: Cu^-_n, Ag^-_n, and Au^-_n. *J. Chem. Phys.* **1990**, *93* (10), 6987−7002.

(27) Taylor, K. J.; Pettiette-Hall, C. L.; Cheshnovsky, O.; Smalley, R. E. Ultraviolet Photoelectron Spectra of Coinage Metal Clusters. *J. Chem. Phys.* **1992**, *96* (4), 3319−3329.

(28) Qu, Z.; Yu, F.; Zhang, X.; Wang, Y.; Gao, J. Support Effects on the Structure and Catalytic Activity of Mesoporous Ag/CeO2 Catalysts for CO Oxidation. *Chemical Engineering Journal* **2013**, *229*, 522−532.

(29) Dutov, V. V.; Mamontov, G. V.; Zaikovskii, V. I.; Liotta, L. F.; Vodyankina, O. V. Low-Temperature CO Oxidation over Ag/SiO2 Catalysts: Effect of OH/Ag Ratio. *Applied Catalysis B: Environmental* **2018**, *221*, 598−609.

(30) Sanchez, A.; Abbet, S.; Heiz, U.; Schneider, W.-D.; Häkkinen, H.; Barnett, R. N.; Landman, U. When Gold Is Not Noble: Nanoscale Gold Catalysts. *J. Phys. Chem. A* **1999**, *103* (48), 9573−9578.

(31) Reber, A. C.; Bista, D.; Chauhan, V.; Khanna, S. N. Transforming Redox Properties of Clusters Using Phosphine Ligands. *J. Phys. Chem. C* **2019**, *123*, 8983−8989.
(32) Chauhan, V.; Reber, A. C.; Khanna, S. N. Strong Lowering of Ionization Energy of Metallic Clusters by Organic Ligands without Changing Shell Filling. *Nat. Commun.* **2018**, *9* (1), 2357.
(33) Sengupta, T.; Khanna, S. N. Converting CO2 to Formic Acid by Tuning Quantum States in Metal Chalcogenide Clusters. *Commun. Chem.* **2023**, *6* (1), 1−9.
(34) Frisch, M. J.; Trucks, G. W.; Schlegel, H. B.; Scuseria, G. E.; Robb, M. A.; Cheeseman, J. R.; Scalmani, G.; Barone, V.; Petersson, G. A.; Nakatsuji, H.; Li, X.; Caricato, M.; Marenich, A.; Bloino, J.; Janesko, B. G.; Gomperts, R.; Mennucci, B.; Hratchian, H. P.; Ortiz, J. V.; Izmaylov, A. F.; Sonnenberg, J. L.; Williams-Young, D.; Ding, F.; Lipparini, F.; Egidi, F.; Goings, J.; Peng, B.; Petrone, A.; Henderson, T.; Ranasinghe, D.; Zakrzewski, V. G.; Gao, J.; Rega, N.; Zheng, G.; Liang, W.; Hada, M.; Ehara, M.; Toyota, K.; Fukuda, R.; Hasegawa, J.; Ishida, M.; Nakajima, T.; Honda, Y.; Kitao, O.; Nakai, H.; Vreven, T.; Throssell, K.; Montgomery, J. A., Jr.; Peralta, J. E.; Ogliaro, F.; Bearpark, M.; Heyd, J. J.; Brothers, E.; Kudin, K. N.; Staroverov, V. N.; Keith, T.; Kobayashi, R.; Normand, J.; Raghavachari, K.; Rendell, A.; Burant, J. C.; Iyengar, S. S.; Tomasi, J.; Cossi, M.; Millam, J. M.; Klene, M.; Adamo, C.; Cammi, R.; Ochterski, J. W.; Martin, R. L.; Morokuma, K.; Farkas, O.; Foresman, J. B.; Fox, D. J.. *Gaussian 09*; 2016.
(35) Ernzerhof, M.; Scuseria, G. E. Assessment of the Perdew−Burke−Ernzerhof Exchange-Correlation Functional. *J. Chem. Phys.* **1999**, *110* (11), 5029−5036.
(36) Wadt, W. R.; Hay, P. J. *Ab Initio* Effective Core Potentials for Molecular Calculations. Potentials for Main Group Elements Na to Bi. *J. Chem. Phys.* **1985**, *82* (1), 284−298.
(37) Laun, J.; Vilela Oliveira, D.; Bredow, T. Consistent Gaussian Basis Sets of Double- and Triple-Zeta Valence with Polarization Quality of the Fifth Period for Solid-State Calculations: Fifth Period for Solid-State Calculations. *J. Comput. Chem.* **2018**, *39* (19), 1285−1290.
(38) Schlegel, H. B. Optimization of Equilibrium Geometries and Transition Structures. *J. Comput. Chem.* **1982**, *3* (2), 214−218.
(39) Li, X.; Frisch, M. J. Energy-Represented Direct Inversion in the Iterative Subspace within a Hybrid Geometry Optimization Method. *J. Chem. Theory Comput.* **2006**, *2* (3), 835−839.
(40) Hirshfeld, F. L. Bonded-Atom Fragments for Describing Molecular Charge Densities. *Theoret. Chim. Acta* **1977**, *44* (2), 129−138.
(41) Reed, A. E.; Weinstock, R. B.; Weinhold, F. Natural Population Analysis. *J. Chem. Phys.* **1985**, *83* (2), 735−746.
(42) Fukui, K. The Path of Chemical Reactions - the IRC Approach. *Acc. Chem. Res.* **1981**, *14* (12), 363−368.
(43) Lu, T.; Chen, F. Multiwfn: A Multifunctional Wavefunction Analyzer. *Journal of computational chemistry* **2012**, *33* (5), 580−592.
(44) Knizia, G. Intrinsic Atomic Orbitals: An Unbiased Bridge between Quantum Theory and Chemical Concepts. *J. Chem. Theory Comput.* **2013**, *9* (11), 4834−4843.
(45) Knizia, G.; Klein, J. E. Electron Flow in Reaction Mechanisms—Revealed from First Principles. *Angew. Chem., Int. Ed.* **2015**, *54* (18), 5518−5522.
(46) McKee, M. L.; Samokhvalov, A. Density Functional Study of Neutral and Charged Silver Clusters Agn with n = 2−22. Evolution of Properties and Structure. *J. Phys. Chem. A* **2017**, *121* (26), 5018−5028.
(47) Baksi, A.; Harvey, S. R.; Natarajan, G.; Wysocki, V. H.; Pradeep, T. Possible Isomers in Ligand Protected Ag $_{11}$ Cluster Ions Identified by Ion Mobility Mass Spectrometry and Fragmented by Surface Induced Dissociation. *Chem. Commun.* **2016**, *52* (19), 3805−3808.
(48) Baksi, A.; Bootharaju, M. S.; Chen, X.; Häkkinen, H.; Pradeep, T. Ag $_{11}$ (SG) $_{7}$: A New Cluster Identified by Mass Spectrometry and Optical Spectroscopy. *J. Phys. Chem. C* **2014**, *118* (37), 21722−21729.
(49) Xie, Y.-P.; Jin, J.-L.; Lu, X.; Mak, T. C. W. High-Nuclearity Silver Thiolate Clusters Constructed with Phosphonates. *Angew. Chem., Int. Ed.* **2015**, *54* (50), 15176−15180.
(50) Lopez-Acevedo, O.; Kacprzak, K. A.; Akola, J.; Häkkinen, H. Quantum Size Effects in Ambient CO Oxidation Catalysed by Ligand-Protected Gold Clusters. *Nature Chem.* **2010**, *2* (4), 329−334.
(51) Boreskov, G. K. *Heterogeneous Catalysis*; Nova Publishers, 2003.
(52) Sinthika, S.; Vala, S. T.; Kawazoe, Y.; Thapa, R. CO Oxidation Prefers the Eley−Rideal or Langmuir−Hinshelwood Pathway: Monolayer vs Thin Film of SiC. *ACS Appl. Mater. Interfaces* **2016**, *8* (8), 5290−5299.
(53) Baxter, R. J.; Hu, P. Insight into Why the Langmuir−Hinshelwood Mechanism Is Generally Preferred. *J. Chem. Phys.* **2002**, *116* (11), 4379−4381.
(54) Wang, Y.; Wu, G.; Yang, M.; Wang, J. Competition between Eley−Rideal and Langmuir−Hinshelwood Pathways of CO Oxidation on Cu $_{n}$ and Cu $_{n}$ O (n = 6, 7) Clusters. *J. Phys. Chem. C* **2013**, *117* (17), 8767−8773.
(55) Zhang, X.; Lu, Z.; Xu, G.; Wang, T.; Ma, D.; Yang, Z.; Yang, L. Single Pt Atom Stabilized on Nitrogen Doped Graphene: CO Oxidation Readily Occurs via the Tri-Molecular Eley−Rideal Mechanism. *Phys. Chem. Chem. Phys.* **2015**, *17* (30), 20006−20013.
(56) Bürgel, C.; Reilly, N. M.; Johnson, G. E.; Mitrić, R.; Kimble, M. L.; Castleman, A. W.; Bonačić-Koutecký, V. Influence of Charge State on the Mechanism of CO Oxidation on Gold Clusters. *J. Am. Chem. Soc.* **2008**, *130* (5), 1694−1698.
(57) Hagen, J.; Socaciu, L. D.; Le Roux, J.; Popolan, D.; Bernhardt, T. M.; Wöste, L.; Mitrić, R.; Noack, H.; Bonačić-Koutecký, V. Cooperative Effects in the Activation of Molecular Oxygen by Anionic Silver Clusters. *J. Am. Chem. Soc.* **2004**, *126* (11), 3442−3443.
(58) Chen, S. F.; Li, J. P.; Qian, K.; Xu, W. P.; Lu, Y.; Huang, W. X.; Yu, S. H. Large Scale Photochemical Synthesis of M@TiO2 Nanocomposites (M = Ag, Pd, Au, Pt) and Their Optical Properties, CO Oxidation Performance, and Antibacterial Effect. *Nano Res.* **2010**, *3* (4), 244−255.
(59) Su, H.-Y.; Yang, M.-M.; Bao, X.-H.; Li, W.-X. The Effect of Water on the CO Oxidation on Ag(111) and Au(111) Surfaces: A First-Principle Study. *J. Phys. Chem. C* **2008**, *112* (44), 17303−17310.
(60) Wang, A.-Q.; Chang, C.-M.; Mou, C.-Y. Evolution of Catalytic Activity of Au−Ag Bimetallic Nanoparticles on Mesoporous Support for CO Oxidation. *J. Phys. Chem. B* **2005**, *109* (40), 18860−18867.
(61) Zhou, Y.; Fuentes-Hernandez, C.; Shim, J.; Meyer, J.; Giordano, A. J.; Li, H.; Winget, P.; Papadopoulos, T.; Cheun, H.; Kim, J.; Fenoll, M.; Dindar, A.; Haske, W.; Najafabadi, E.; Khan, T. M.; Sojoudi, H.; Barlow, S.; Graham, S.; Brédas, J.-L.; Marder, S. R.; Kahn, A.; Kippelen, B. A Universal Method to Produce Low−Work Function Electrodes for Organic Electronics. *Science* **2012**, *336* (6079), 327−332.
(62) Ford, W. E.; Gao, D.; Knorr, N.; Wirtz, R.; Scholz, F.; Karipidou, Z.; Ogasawara, K.; Rosselli, S.; Rodin, V.; Nelles, G.; von Wrochem, F. Organic Dipole Layers for Ultralow Work Function Electrodes. *ACS Nano* **2014**, *8* (9), 9173−9180.
(63) Lang, N. D. Theory of Work-Function Changes Induced by Alkali Adsorption. *Phys. Rev. B* **1971**, *4* (12), 4234−4244.
(64) Roberts, F. S.; Anderson, S. L.; Reber, A. C.; Khanna, S. N. Initial and Final State Effects in the Ultraviolet and X-Ray Photoelectron Spectroscopy (UPS and XPS) of Size-Selected Pd $_{n}$ Clusters Supported on TiO $_{2}$ (110). *J. Phys. Chem. C* **2015**, *119* (11), 6033−6046.
(65) Watanabe, T.; Koyasu, K.; Tsukuda, T. Density Functional Theory Study on Stabilization of the Al $_{13}$ Superatom by Poly(Vinylpyrrolidone). *J. Phys. Chem. C* **2015**, *119* (20), 10904−10909.

https://doi.org/10.1021/acs.jpca.3c04675
J. Phys. Chem. A 2023, 127, 10766−10774